Angiogenic responses in a 3D micro-engineered environment of primary endothelial cells and pericytes

As Published: https://doi.org/10.1007/s10456-020-09746-6

Publisher: Springer Netherlands

Persistent URL: https://hdl.handle.net/1721.1/132011

Version: Author's final manuscript: final author's manuscript post peer review, without publisher's formatting or copy editing

Angiogenic responses in a 3D micro-engineered environment of primary endothelial cells and pericytes

Cite this article as: Jing Bai, Mehrdad Khajavi, Lufei Sui, Haojie Fu, Subrahmanian Tarakkad Krishnaji, Amy E. Birsner, Lauren Bazinet, Roger D. Kamm and Robert J. D'Amato, Angiogenic responses in a 3D micro-engineered environment of primary endothelial cells and pericytes, Angiogenesis https://doi.org/10.1007/s10456-020-09746-6

Angiogenic responses in a 3D micro-engineered environment of primary endothelial cells and pericytes

Jing Bai[1,3]*, Mehrdad Khajavi[1], Lufei Sui[1], Haojie Fu[1], Subrahmanian Tarakkad Krishnaji[1], Amy E. Birsner[1], Lauren Bazinet[1], Roger D. Kamm[3] and Robert J. D'Amato[1,2]

[1]The Vascular Biology Program and Department of Surgery, Boston Children's Hospital, Harvard Medical School, Boston, Massachusetts, United States of America;

[2]Department of Ophthalmology, Harvard Medical School, Boston, Massachusetts, United States of America;

[3]Department of Mechanical Engineering, Massachusetts Institute of Technology, Cambridge, Massachusetts, United States of America.

* baij0005@e.ntu.edu.sg

Key Words: Microfluidic, Angiogenesis, Primary endothelial cell, Pericyte, 3D cell culture

Abstract

Angiogenesis plays a key role in the pathology of diseases such as cancer, diabetic retinopathy and age-related macular degeneration. Understanding the driving forces of endothelial cell migration and organization, as well as the time frame of these processes, can elucidate mechanisms of action of important pathological pathways. Herein, we have developed an organ-specific microfluidic platform recapitulating the *in vivo* angiogenic microenvironment by co-culturing mouse primary brain endothelial cells with brain pericytes in a three-dimensional (3D) collagen scaffold. As a proof of concept, we show that this model can be used for studying the angiogenic process and further comparing the angiogenic properties between two different common inbred mouse strains, C57BL/6J and 129S1/SvlmJ. We further show that the newly discovered angiogenesis-regulating gene *Padi2* promotes angiogenesis through *Dll4/Notch1* signaling by an on-chip mechanistic study. Analysis of the interplay between primary endothelial cells and pericytes in a 3D microfluidic environment assists in the elucidation of the angiogenic response.

Introduction

Angiogenesis is the process of forming new capillary vessel sprouts from an existing blood vessel. The process plays a critical function during development and in a number of diseases such as cancer, cardiovascular disease, and age-related macular degeneration. Complex signaling networks are involved in regulating angiogenesis and therapeutic targets have been discovered either to stimulate or to suppress these networks. The most well-known stimulator is vascular endothelial growth factor (VEGF), an angiogenic factor that acts in a concentration-gradient driven manner. The VEGF family has many members but VEGF-A plays the most important role in endothelial responses[1-4]. This growth factor stimulates robust chemotaxis in which endothelial cells migrate from low to high VEGF-A concentration. VEGF-A is essential for the induction and growth of angiogenic tip cells through the Notch signaling pathways [2,5]. Notch signaling pathways are evolutionarily conserved and determine cell fate and differentiation. They are activated via cleavage of Notch intracellular domain (NICD) by γ-secretase, causing the translocation of NICD to the nucleus in which it regulates transcription of its target genes[6]. Notch signaling through *Notch1* and *Notch4* plays a key role in angiogenesis and is regulated by several Notch ligands including *Dll1, 2, 4,* and *Jagged1, 2* [7]. During angiogenesis, *Dll4* and *Jagged1* have different roles [8]. In response to VEGF, *Dll4* is mainly expressed on angiogenic tip cells that make up the leading front of the vascular sprout. *Dll4* expression defines tip cell identity by regulating expression of cell surface receptors such as VEGFR-2/3, NRP1, and PDGF-BB. In addition, *Dll4* expression in tip cells suppresses the tip phenotype in neighboring endothelial cells wherein stalk cells become new tip cells. *Jagged1* promotes proliferation and sprouting phenotype by antagonizing *Dll4/Notch* signaling. The balance and specific selection of ligand binding to Notch receptors among endothelial cells are still not clear [8].

Although cell-based models play a key role in biomedical research and drug discovery, most *in vitro* 2D cell models do not adequately address the topology of the tissue components, reducing their ability to recapitulate the *in vivo* processes. 3D cultures better mimic *in vivo* growth and interaction with the surroundings, as well as polarization and differentiation [9]. Collagen which is derived from intrinsic extra-cellular matrix (ECM) has a high-level of biocompatibility and can be employed [10] to facilitate cellular adhesion and support the interplay between cells and their stroma. Despite the advantages of *in vivo* systems, most models lack high-throughput capability and are time consuming.

Microfluidic cell-based 3D models complement *in vivo* systems by providing a more streamlined approach, while implementing complexities not achievable in 2D *in vitro* systems[11-13]. These 3D models have been utilized for a number of different cell culture applications, with advantages of real-time imaging in a controlled geometrical, physical and biochemical microenvironment [14-16]. Previous reports of microfluidic cell-based 3D models used in studying angiogenesis involve spatial control, lumen formation, gradient formation and perfusion for vasculature applications [17-20] as well as interaction with different types of tissues [21-23]. However, these microfluidic cell culture models mainly rely on transformed cell lines that have been previously propagated outside of their physiological environment for an extended time, and thus may not be useful for particular applications due to accumulating genetic alterations during passaging and contamination by other aggressive cell types [24]. While primary cells have a limited life span, they benefit from functional and genetic fidelity [25]. Thus, primary cells will be of better use to study heterogeneous cells isolated from different tissues, or different genetic backgrounds. In addition, endothelial cell lines isolated from various tissues behave differently in terms of their junction complexes, endothelium fenestra, morphology and permeability [1]. Hence, it is important to isolate tissue-specific endothelial cells to re-capitulate the *in vivo* micro-physiological systems of interest.

To allow maximum preservation of *in vivo* signaling networks, herein we describe a 3D microfluidic construct with primary endothelial cells and co-cultured pericytes isolated simultaneously from murine brain tissue. We used this model system to study angiogenesis in two strains of mice with different genetic backgrounds. We have previously shown that the ability to respond to angiogenic stimuli is controlled by genetic variation[26] and performed genome-wide association studies (GWAS) in common inbred mouse strains to identify novel genes responsible for differences in angiogenic response [27]. Peptidyl arginine deiminase type 2 (*Padi2),* whose involvement has been linked to many human diseases such as cancer[28] and neurodegenerative diseases,[29] has been recently identified as a novel angiogenesis-regulating gene. Using our 3D microfluidic construct, here we derived primary endothelial cells and pericytes from either a “high (129S1/SvlmJ)” or a “low (C57BL/6J)” angiogenic strain [26,27]. As a proof of concept, we examined the differences in angiogenic response to VEGF. The potential mechanism of Padi2 was also investigated using our novel microfluidic system.

Understanding these processes can aid and expand our knowledge of the pathways that directly mediate angiogenic response.

Results

Isolation of primary murine brain endothelial cells and pericytes to mimic 3D angiogenic microenvironment

We successfully isolated and cultured primary brain endothelial cells from C57BL/6J and 129S1/SvlmJ and used these cells to create a three-dimensional angiogenic microenvironment. Figure 1a is a descriptive flow chart for cell culture preparations. We improved the existing method [30] for optimizing the cell yield and survival as described in the Method section. Puromycin selection was used to eliminate all other cell types while selecting only for brain endothelial cells expressing P-glycoprotein[31]. The same starting culture system was used for growing pericytes. However, as pericytes were passaged, they outgrew endothelial cells and become dominant in the culture. To verify endothelial cells and pericytes, we examined the expression of two specific markers for both endothelial cell (CD31 and VEGFR2) and pericytes (PDGFRβ and NG2) via flow cytometry analyses. While there is no specific marker available to identify pericytes, usually a combination of markers of NG2 and PDGFRβ is used to phenotype these cells. Our results showed that over 95% and 92% of isolated primary brain endothelial cells express high levels of CD31 and VEGFR2, respectively, and over 89% and 81% of pericytes express high levels of PDGFRβ and NG2, respectively (Figure 1b). In flow cytometry analysis, the two types of cells behaved distinctively different from one another. The cell purity was similar with the existing method [30]; however, the brain endothelial cell number based on our method was increased 1.6 times higher than current methods[30] (Gating strategy shown in Supplementary Figure 1). We confirmed this by immunostaining the cells using their specific markers CD31 and NG2, respectively (Figure 1c). Cell morphology is shown in Figure 1d.

For this study, a previously reported microfluidic system (Figure 1e)[22] was used with minor changes. Primary endothelial cells and pericytes were seeded together in the fluidic channel and allowed to assemble in order to mimic the vascular capillary structure (pericyte migration shown in Supplementary Figure 2). In this study, we also optimized the pericyte to endothelial cell ratio (Supplementary Figure 3) to 1:20. Approximately 30,000-50,000 endothelial cells and 1,500-

2,000 pericytes per device were seeded. After 7 days of VEGF stimulation, vessel sprouts started to grow into the central collagen gel channel. Along with vessel growth, pericytes were recruited and migrated along the surface of new sprouts (Figure 1e). This system mimics physiological angiogenesis (Figure 1f). Initially, blood vessels are covered with pericytes and a single pericyte can interact with multiple endothelial cells. In the presence of VEGF-A, pericytes start to detach from the migrating tip cells (arrow), then the endothelial cells sprout as filopodial-like structures followed by tube formation. Eventually, pericytes migrate along the endothelial tubes and stabilize them.

C57BL/6J and 129S1/SvlmJ isolated endothelial cells and pericytes respond differently to angiogenic stimuli

After cells were seeded in the devices, pericytes and endothelial cells self-organized into lumen-like structures at 12 h post-seeding. Visualization of pericytes revealed that they were localized surrounding these tubular structures, rather than forming a mosaic monolayer. Initially the endothelial cells formed a single layer (red layer) surrounded by pericytes (green layer). The results demonstrate the setup has the correct configuration of an inner lining of ECs and outer lining of PCs (Figure 2a, a 3-sction view image was shown in Supplementary Figure 4). The presence of pericytes also influence the functionality of the system via formation of vascular plexus and continuous endothelium, which is required for developing mature vasculature (Supplementary Figure 5). We have previously shown that there are significant differences in angiogenic response among different common inbred strains and demonstrated that this trait is genetically controlled by different loci [27]. Here, as a proof of concept we compared the angiogenic response of primary endothelial cells isolated from two different strains, C57BL/6J and 129S1/SvlmJ with different angiogenic responsiveness. Endothelial cells isolated from the high angiogenic strain, 129S1/SvlmJ, exhibited a higher level of angiogenesis in terms of sprouting length, tip cell numbers and average vessel diameters when compared to C57BL/6J (low angiogenic) (Figure 2b; Supplementary Figure 6 for phase-contrast image comparison). In both the isolated endothelial cell culture as well as the co-culture with pericytes system, the sprout length of medium sized vessels from the 129S1/SvlmJ was approximately 1.6-fold higher compared to the C57BL/6J in response to VEGF (Figure 2c). The average tip cell numbers in 129S1/SvlmJ was likewise higher than C57BL/6J (11±2.2 vs. 7±1.7) in the absence of

pericytes and also when co-cultured with pericytes (14±2.6 vs. 9±2.8, Figure 2d). Vessels comprised of endothelial cells from C57BL/6J or 129S1/SvlmJ showed similar diameters (16.6 µm and 17.0 µm, respectively). However, when these cells were co-cultured with their respective pericytes, a slightly larger vessel diameter (1.25 fold) was observed in 129S1/SvlmJ compared to C57BL/6J (Figure 2e). In flow conditions, we have also observed this trend of angiogenesis in C57BL/6J versus 129S1/SvlmJ endothelial cells (Supplementary Figure 7, Supplementary Methods), as VEGF works together with mechanical fluid forces to mediate angiogenesis[32]. To mimic the physiological shear stress subjected by blood vessels (5-10 dyn/cm^{2,} post capillary venules to arteries[33]), the flow rate was set to 1000 µl/h, giving the existing flow channel height and width (See Supplementary Figure 7).

Pericyte recruitment and endothelial vessel lumen formation is depicted in a 3-section view in figure 2f. The white arrow identifies a new vessel with formed intact lumen (red) that is surrounded by a few pericytes (green). Vessel permeability was quantified by testing the diffusion pattern of 70 kDa dextran rhodamine (Figure 2g). A decrease in fluorescence intensity indicated the presence of a barrier. As expected, vessels formed by endothelial cells alone showed significantly more leakage than vessels formed by co-cultured endothelial cells and pericytes. However, there was no difference in permeability between C57BL/6J and 129S1/SvlmJ under either condition (Figure 2h, calculation of diffusive permeability shown in Supplementary Method). However, 129S1/SvlmJ exhibited a higher level of angiogenesis with more migration of endothelial cells and pericytes (Figure 2i, j, k).

High PADI2 expression in endothelial cells and angiogenic tip cells from 129S1/SvlmJ

We found that PADI2 is expressed at higher levels mainly in the primary endothelial cells from high angiogenic mouse strain 129S1/SvlmJ when compared to C57BL6/J (Figure 3a). This is consistent with the *in vivo* finding in murine corneal models [20]. Higher PADI2 expression was found in the tip cells for both strains (Figure 3a), but more prominent in the 129S1/SvlmJ. Similar observation with endothelial cells alone is shown in Supplementary Figure 8. Figure 3b demonstrates the presence of the VEGF enhanced PADI2 expression in endothelial cells from both C57BL/6J and 129S1/SvlmJ. Notably, in the absence of VEGF with minimal vessel sprouting, PADI2 expression was also minimal, suggesting PADI2 expression may be induced by VEGF and may also play a role in the angiogenic tip cell phenotype. Notably, no difference

was observed on PADI2 expression in the presence of flow compared to static condition (Supplementary Figure 9).

PADI2 inhibition reduces angiogenesis in a 3D system

In order to determine whether PADI2 expression levels affect angiogenesis in a 3D system, we assessed the effect of *Padi2* knockdown by siRNA using electroporation. The knockdown process is demonstrated in Supplementary Figure 10. Figure 4a shows significant *Padi2* knock-down on 129S1/SvlmJ primary endothelial cells. We observed significant reduction in vessel sprouting length (94.3 μm vs. 63.2 μm), tip cell numbers (9±2.0 vs. 4±1.4) and vessel diameters (22.8 μm vs. 11.1 μm) in siRNA treated groups compared to vehicle control (Figure 4b, c, d and e). We then treated the primary endothelial cells in the 3D assay with BB-Cl-Amidine, a potent inhibitor of PADI2, and found a significant decrease in sprouting length (Figure 4g), number of tip cells (Figure 5h) and vessel diameters (Figure 4i) in a dose dependent manner. This drug was tested at multiple concentrations in both 3D assays (Figure 4f) and in standard 2D cell culture (Figure 4j) to determine the concentration needed to produce adequate inhibition. We observed the largest effect of BB-Cl-Amidine with no toxicity at a concentration of 500nM in the 3D assay (Figure 4f). In standard cell culture, a significantly impaired endothelial cell monolayer is present at 1μM. The results suggest that *Padi2* is involved in angiogenesis through regulating tip cell formation and migration. Interestingly, pericyte migration pattern in BB-Cl-Amidine treated group was similar with control group, with pericytes still migrating along vessel sprouting trunks (Figure 4 k, l). However, pericytes migration distance was reduced in the BB-Cl-Amidine treated group compared to control, which is likely due to the inhibition of endothelial cell migration. Among all the PADIs, *Padi2* and *Padi4* are the most common isoforms in brain tissue and were shown to have nuclear activity [34]. To exclude any effect of *Padi4*, we performed immunostaining of *Padi4* in BB-Cl-Amidine and DAPT treatment groups (Supplementary Figure 11A) and found no change in PADI4 expression compared to corresponding control groups. *Padi4* siRNA knockdown also did not affect the phenotype of angiogenesis (Supplementary Figure 11B and 11C). These results suggest that *Padi4* is not involved in angiogenesis regulation in this system.

PADI2 expression is up-regulated when Notch signaling pathway is inhibited

Due to high expression of PADI2 in tip cells, we investigated if there was a possible interplay between PADI2 expression and Notch signaling. Notch signaling is known to play an important role in angiogenesis by regulating differentiation of tip cells and stalk cells[35]. In the presence of VEGF stimulation, Notch signaling is involved in a complex crosstalk between tip cells and stalk cells in creating a new branching point [2]. C57BL/6J primary endothelial cells treated with γ-secretase inhibitor N-[N-(3,5-Difluorophenacetyl)-L-alanyl]-S-phenylglycine t-butyl ester (DAPT) resulted in an elevated level of PADI2, specifically more significant in the enlarged tip cell regions compared to an untreated group (Figure 5a). We found similar results in endothelial cells treated with DAPT from 129S1/SvlmJ mice (Figure 5b). PADI2 appeared to accumulate in the tip cell regions in DAPT treated group (Figure 5c). We next assessed the level of citrullination (a byproduct of Padi enzymatic activity) in these cells and found a correlation (Figure 5a, 5c). Interestingly, PADI2 expression in the tip cell nuclei was absent when treated with DAPT together with BB-Cl-Amidine treatment. In previous, PADI2 was detected in the nucleus and cytoplasm and has been found to citrullinate nuclear histone and several RNA binding proteins, thus regulating transcription through epigenetic mechanisms[36,37]. This may suggest that Notch signaling is associated with PADI2 expression (Figure 5c).

Padi2 promotes angiogenesis through crosstalk with *Dll4/Notch1* signaling pathway

To elucidate the role of Notch signaling and *Padi2*-related pathways in angiogenesis, Notch1 intracellular domain (N1ICD) level was evaluated in the sprouting vessel branches (*Padi2* knockdown endothelial cell from 129S1/SvlmJ mice). N1ICD was upregulated in both *Padi2* knockdown cells and BB-Cl-Amidine treated cells compared to the corresponding control groups (Figure 6a), and increased N1ICD levels in the nuclei were also observed by immunofluorescence (Figure 6b). In addition, the expression of Notch downstream genes Hey1 and Hey2 was upregulated in the sprouting vessel branches in the *Padi2* knock-down group (Figure 6c and enlarged view, 6d), indicating Notch signaling was elevated when PADI2 was inhibited. Figure 6e shows that DAPT abolished the BB-Cl-Amidine effects by restoring sprouting formation (Figure 6d), the number of tip cells (Figure 6e) and vessel diameters (Figure 6f and 6g), in comparison to control. Figure 6h was representative image for each group.

To investigate the effect of Notch ligands, we examined *Dll4, Jagged1* and *Dll1*. We observed a slightly higher DLL4 expression in the BB-Cl-Amidine treated group (Figure 7a, Figure 7b),

while JAGGED1 and DLL1 expression showed no significant differences by either Western blot or immunostaining. We then examined the effect of applied recombinant mouse DLL4 protein. An overview of neovascular stabilization and morphogenesis is shown in Figure 7c. The DLL4-stimulated group had reduced sprouting length (Figure 7d), vessel diameter (Figure 7e), and fewer tip cell numbers (Figure 7f) compared to untreated endothelial cells. Additional BB-Cl-Amidine treatment further reduced sprouting angiogenesis. However, DAPT treatment counters the effects of inhibiting PADI2.

Discussion

In this study, we created a novel 3D microfluidic angiogenic model with primary mouse brain microvascular endothelial cells and pericytes. With this model, we compared *in vitro* sprouting angiogenesis using cells derived from two inbred mouse strains to investigate the mechanisms behind the differences reported in their angiogenesis *in vivo*. A key inspiration for our investigation was to develop a 3D *in vitro* system to recapitulate different angiogenic phenotypes observed *in vivo*. Lack of complex cellular and structural microenvironments in conventional 2D *in vitro* assays poorly replicates the desired phenotypes. Furthermore, this microfluidic-based platform is capable of validating candidate genes identified by GWAS *in vitro* by performing mechanistic studies.

In a previous study, we addressed the genetic contribution to different responses of angiogenesis in mouse models. In this study, we have isolated microvascular endothelial cells and pericytes from the same organ to capture the unique angiogenic microenvironment that is lost within non-primary cells and cells from different tissues. We selected brain tissue for our 3D angiogenesis model, in part, because pericytes and microvascular endothelial cells are abundantly present in the brain microvasculature and are well-differentiated. Most importantly, cerebrovascular disease such as stroke[38] is one of the most prevalent life-threatening diseases world-wide. Successfully development of a primary endothelial cell-based, central nervous system (CNS) vascular model would benefit future studies of CNS vascular diseases. We have improved the current methods in isolating mouse primary endothelial cells from brain by using a different enzyme for digestion and modifying the protocols as mentioned in the Methods section. Our improved protocol has increased the recovery of primary endothelial cells growing in microfluidic devices.

We have previously shown that 129S1/SvlmJ mice exhibit more robust angiogenesis compared to C57BL6/J in response to growth factors bFGF and VEGF in a corneal micropocket assay[27]. Here, we find that 129S1/SvlmJ endothelial cells are highly angiogenic characterized by elongated, enlarged vessels, and increased numbers of tip cells under both static and flow conditions. From our results, pericytes had minimal effect on alternating sprouting trends in both strains, but they played a key role in stabilizing lumen-like vessel structures in our system and employed an essential role on endothelial cell proliferation, migration and stabilization. They assist in developing the vessel plexus by initiating vascular anastomoses. As well, pericytes reinforce vascular structures via forming continuous endothelium with noninterrupted stress fibers. In addition, they prevent vessel leakage while promote vessel maturation, similar to previous reports that pericytes play a key role in controlling cerebral perfusion and restricting the brain microvasculature permeability [39,40]. Notably, our system with endothelial cells and pericytes recapitulates the basic unit of vasculature and mimics physiological angiogenesis through the process of pericyte detachment, tip cells migration, pericytes re-adhesion and pericyte migration following neovessel sprouts. We concluded that pericytes are essential in the 3D systems to retain normal vessel function in order to mimic angiogenesis process.

Padi2 is part of the peptidyl arginine deiminase family of enzymes that catalyze the post-translational conversion of peptidyl arginine residues to citrulline in the presence of Ca^{2+}[41]. Padi2 has shown to be involved in tumor progression[42] and neurodegenerative human disorders including Alzheimer's disease and multiple sclerosis[43]. We recently showed the potential role of *Padi2* as an angiogenesis-regulating gene[27]. Herein, we recapitulated the unique *in vivo* vascular microenvironment *in vitro* in order to study the function of *Padi2* in a simpler system. In addition, we were able to perform cell specific knock-down experiments on endothelial cells which is more difficult to achieve in animal models. In this 3D model, PADI2 inhibitor inhibited angiogenesis in a dose dependent manner.

The connection between *Padi2* and Notch signaling has not been previously explored. Here, we found PADI2 expression higher in endothelial tip cells compared to stalk cells (non-tip cells) in the presence of VEGF. We then found a strong association between Notch signaling and PADI2 expression in our model. In both *Padi2* knock-down and BB-Cl-Amidine treated endothelial cells, N1ICD was elevated compared to the corresponding controls. This resulted in reduced

sprouting angiogenesis in both strains tested in this study. This reduced angiogenic phenotype was abrogated by blocking Notch signaling. Our results reveal a previously unknown *Padi2* endothelial function through crosstalk with *Dll4/Notch1* signaling. Previous studies have shown that *Dll4/Notch1* signaling inhibition leads to increased filopodia protrusion and vessel diameter in animal studies [44]. In addition, angiogenesis requires a tightly coordinated balance between EC sprouting (tip cells) and the maintenance of existing vasculature (stalk cells)[8] and this balance can be controlled by *Dll4* expression in endothelial tip cells [2,45]. Here, our observation indicated that when *Padi2* is highly expressed, it leads to lower levels of *Dll4* in the stalk cells resulting in an angiogenic "shift" toward a more proangiogenic state. Our results suggest that high *Padi2* expression in 129S1/SvlmJ may be partially responsible for the high angiogenic response due to its involvement of *Dll4/Notch1* signaling in the regulation of sprouting. We found that down-regulation of *Padi2* correlated with higher *Dll4/Notch1* signaling and resulted in N1ICD being released, which led to reduced tip cell formation and lower angiogenesis. In contrast, up-regulation of *Padi2* resulted in lower *Dll4/Notch1* signaling with increased tip cell formation and accelerated angiogenesis. Based on our data, N1ICD is up-regulated when Padi2 was knocked down. This may be due to Padi2 being involved in Notch cleavage and the release of N1ICD, followed by the activation of Notch signaling and increased N1ICD nuclei translocation. Future studies are required to show the detailed mechanism of Padi2 involvement in Notch signaling pathway.

In this study, a continuum of pericyte cellular phenotype and lack of a specific pericyte marker was a limitation of primary pericyte isolation from passage 1. However, we still believe this primary-cell-based microfluidic prototype is useful to study cellular mechanisms and to address the complex interplay of networks via multi-cellular microenvironment settings. Future work will investigate further the reciprocal role of *Padi2* and Notch signaling. This microfluidic vasculature surrogate facilitates the study of potential pathways involved in angiogenic response. In addition, many studies develop personalized therapies via customizing genetic interventions within genetic models. Murine models are feasible to study specific gene mutations; however, one can use the primary murine cells from specific tissues with various phenotypic features to investigate disease mechanisms which has potential for personalized medicine.

Conclusions

This study describes a microfluidic-based platform, integrating primary endothelial cells and pericytes isolated from the same organ. We have compared the genetic differences between mouse strains and investigated the interaction between angiogenic stimuli and cellular responses through a high-resolution confocal imaging. Herein, we have shown that *Padi2*, a novel angiogenesis gene recently identified in a mouse GWAS study, is highly expressed in angiogenic tip cells and interacts with VEGF-A and Notch signaling pathways. Further, a possible mechanism for this effect appears to be through *Padi2* association with the *Dll4/Notch1* signaling pathway. Our model enables the investigation of genetic phenotypes in a 3D microphysiological system and further elucidates the role of *Padi2* in angiogenesis.

Methods

Mouse Primary Endothelial Cells/Pericyte Isolation and Culture

Primary cultures of mouse brain capillary endothelial cells were prepared from 7-week-old mice. Briefly, 4-5 mice were euthanized via CO_2 and brain tissue was minced under aseptic conditions into approximately 1 mm^3 pieces. The pulp was digested for 1h in 37 °C using 9 mL of 1 mg/mL Collagenase A (Roche) with 40 μg/mL *DNase-I*, prepared in an ice-cold Dulbecco's modified Eagle's medium (DMEM). The mixture was then dissociated by approximately 25 gentle inversions. The cell pellet was separated by centrifugation in 14-15 mL of 20% bovine serum albumin (BSA)-PBS (2000 rpm, 15 min with soft deceleration setting). After that, the cell pellet was further digested with 5 mL additional enzyme (same as above) for another 15 min in 37 °C. Digestion was stopped by neutralizing with 5 mL Fetal Bovine Serum (FBS) and centrifuged for 5 min (2000 rpm). The harvested endothelial cells were grown in two 75 cm^2 tissue culture flasks (pre-coated with 1% BD collagen-I and dissolved in 0.02 N acetic acid), and EGM-2MV media (Lonza) with 20% vol/vol FBS and 1x pen-strep for overnight. Cells were maintained in fresh cell culture media on the second day with additional 3 μg/mL puromycin (final concentration) for 3 days. The media was changed every other day. At day 5, cells were grown in fresh media without puromycin for 24 h and were harvested with 0.05% Trypsin-EDTA on day 6 for culturing on microfluidic devices. For primary pericytes, the culture steps were identical except for puromycin was omitted, and FBS concentration was 5% vol/vol in the culture media. After passage 2, cells were maintained in a mouse pericyte media with 2% FBS (Sciencell) and used from passage 5-8.

Microfluidic Device Fabrication and Angiogenesis Microenvironment Generation

The microfluidic device for this study was fabricated using polydimethyl siloxane (PDMS). The PDMS replica was made by soft lithography from SU-8 patterned wafers. The device has one gel channel in the middle and two outer fluidic channels. A coverslip was washed with glacial acetic acids for 1 h, then washed with DI water and ethanol before bonded to the micropattern to form a closed chamber. The endothelial cell/pericyte-growth channel was formed via injection of collagen gel solution (Invitrogen, 2.5 mg/mL. pH 7.4) in the central channel. After gelation, cell growing channel was coated with 50 µg/mL collagen IV (Sigma-Aldrich) and incubated in 37 °C for at least 1/2 h before washed 3 times with DI water and air dried. endothelial cells ($6x10^5$ cells/mL) and pericytes ($1.2x10^5$ cells/mL) were mixed in the ratio of 5:1 and were attached to one of the fluidic channels with the device flipped vertically for 30 min. By flipping the device back, endothelial cells ($3x10^6$ cells/mL) were then seeded again to form a semi-confluent monolayer on the coverslip bottom substrate and onto the gel surface. On day 2, angiogenesis was induced by applying 25 ng/mL recombinated human VEGF 165 (R&D Systems, 293-VE-010) on the other fluidic channel, creating a VEGF concentration gradient across the channels. Media was changed everyday for 7 days to maintain the concentration gradient.

Characterization of Endothelial Cell-Pericyte Coculture Permeability

Fluorescent dextran 70 kDa Texas Red (Life Tech, D-1830) was added to culture media at 12.5 µg/mL[46]. The mixture was applied to the endothelial cell channel. Using fluorescence microscopy, the concentration fields were captured at 0 min and 5 min, respectively (No flow was applied during a permeability measurement). Their raw intensity profiles were analyzed using ImageJ (LOCI, University of Wisconsin). Permeability calculation was described in Supplementary Method.

Electroporation

Primary endothelial cells were washed with PBS, harvested with Trypsin-EDTA, and suspended 100 µL in Nucleofector™ Solution in a cell density of 7×10^5 cells with or without siRNA (On-target smart pool siRNA for mouse *Padi2*, 300 nM, Dharmacon). The RNA-cell mixtures were transferred into cuvettes provided in Basic EC Nucleofector Kit (Lonza), and electroporated using pre-set conditions for endothelial cells in Nucleofector™ 2 Devices (Lonza). After

transfection, EGM-2MV media was added and cells were immediately replated into the microfluidic device.

Immunocytochemistry of cells

Primary endothelial cells and pericytes were stained with CD31 (BD Biosciences, 553373), NG2 (Millipore, AB5320), PADI2 (ProteinTech, 12110-1), citrulline (Fisher Scientific, MABN328), PDGF-BB (LSBio, LS-C201038) NOTCH1 intracellular domain- N1ICD (Novus Biologicals, NB100-78486), Hey1 (Abcam, ab154077), Hey2 (Abcam, ab167280), JAGGED1 (Abcam, ab109536), DLL1 (Abcam, ab85346) and DLL4 (ProteinTech, 21584-1). Briefly, cell culture media was removed from the fluidic channels, and the channel containing the cells was rinsed in PBS and fixed in 4% Paraformaldehyde (PFA) (Sigma-Aldrich) for 15min at room temperature. 0.1% Triton X-100 (Sigma-Aldrich) was then added for 15 min before blocking by 5% BSA dissolved in 1xPBS for 45 min-1 h at room temperature. After that, the cells were stained with primary antibodies (1:100) overnight at 4 °C. Secondary antibodies (1:200), Alexa Fluor 488 (goat anti rabbit IgG (H+L), Invitrogen), or Alexa Fluor 647 (goat anti mouse IgG (H+L)) were added for 1 h at room temperature as needed. Fluorescent images were obtained by confocal microscopy (Zeiss LSM880). For stimulating Notch signaling, recombinant mouse DLL4 protein was used at 10 µg/mL (R&D Systems, 1398-D4-050).

Image Processing and Analysis

Three-dimensional image stacks (80 µm range) of individual endothelial cell sprouts were acquired by confocal microscopy using a 20x objective lens. Images of sprouting length, tip cell numbers and vessel diameters were quantified by Imaris 7.0 software (Bitplane) and ImageJ (LOCI, University of Wisconsin). Sprouting length was defined by the distance of the tip of the furthest migrated cells to the trunk vessel for every individual sprout in a particular region. A region was defined by one 20x image view containing two collagen spaces in between of every three pillars, and tip cell number was quantified within a region. Quantification of vessel diameter was performed by analyzing individual skeletonized 3D projection images using ImageJ plugin AnalyzeSkeleton of the average diameter in a region. Estimated vessel diameter was obtained by dividing area of capillary sprouting by skeletal length.

Flow Cytometry

Primary endothelial cells and pericytes were harvested by 0.05%Trypsin-EDTA and were washed once with PBS and resuspended in FACS buffer (PBS containing 5% (vol/vol) BSA). They were then stained with fluorochrome-conjugated Abs for 1h at room temperature. Labeled cells were washed once with PBS and analyzed using BD FACS Calibur (BD Biosciences). Cells were also stained with isotype-matched antibodies to exclude background staining. All data were analyzed by the FlowJo software (Tree Star Inc.). The antibodies used in this study PE-conjugated CD31 (BD Biosciences, 553373), FITC conjugated PDGFR-β (Santa Cruz, sc-432), PE conjugated VEGFR2 (R&D Systems, FAB357P), and NG2 (Abcam, AB5320) + Alexa Fluor 488 (goat anti rabbit, IgG (H+L), Invitrogen), all with the ratio of 1:100.

Western Blot

Total protein lysates extracted from primary endothelial cell cultures were used in western blot analysis. Protein separation was performed using 12% SDS-PAGE and transferred to nitrocellulose membrane. Non-specific binding was blocked by 3% non-fat milk in Tris-buffered saline (TBS; 25 mM Tris, 150 mM NaCl, 2 mM KCl, pH 7.4) containing 0.1% Tween-20. Primary antibodies were used at 1:1000 to incubate blots overnight at 4 °C, including PADI2 (ProteinTech, 12110-1) JAGGED1 (Abcam, ab109536), DLL1 (Abcam, ab85346) and DLL4 (ProteinTech, 21584-1). Peroxidase-conjugated anti-mouse, anti-rabbit and anti-goat immunoglobulins (GE Healthcare) were used as secondary antibodies. The developed X-ray film was then scanned using Densitometer (Bio-Rad) and analyzed using QualityOne software (Bio-Rad). Western blotting was performed on two individual sets of designed experiments– One was to determine *Padi2* knock-down level, the other was to examine DLL4 expression on BB-Cl-Amidine treatment.

Statistical Analysis

All data are expressed as mean ± S.E.M. Comparison between multiple groups was performed by one-way-ANOVA and indicated by following Tukey means comparison tests. Unpaired Student's t test was used when comparing two groups (defined as: * $p<0.05$; ** $p<0.01$; **** $p<0.0001$). Analysis performed by Prism 7 (GraphPad). All measurements were calculated by averaging the mean values of at least three microfluidic devices, obtained at least two independent experiments with at least 3 measurements made for each device.

Declaration

Funding: This study was supported, in part, by the NIH National Eye Institute. Award Number R01EY012726-12 (to RJD)

Conflict of Interest: The author(s) declare(s) that there is no conflict of interest regarding the publication of this article.

Ethics Approval: All animal studies were conducted in compliance with the protocols approved by the Institutional Animal Care and Use Committee of Boston Children's Hospital (approval number 15-08-2998R for mouse experiments).

Availability of Data and Materials: All data generated or analyzed during this study are included in this article (and its supplementary information files), are available from the corresponding author upon request.

Code Availability: N.A.

Authors Contributions: J.B., R.J.D., M.K., HJ.F., S.T.K., A.E.B. contributed to the design and implementation of the research, J.B., LF.S. and L.B. performed the experiments, and J.B. R.J.D. R.D.K. and M.K. contributed to the interpretation of the results and the preparation of the manuscript. All authors provided critical feedback and helped shape the research, analysis and manuscript.

References

1. Craig LE, Spelman JP, Strandberg JD, Zink MC (1998) Endothelial cells from diverse tissues exhibit differences in growth and morphology. Microvascular research 55 (1):65-76. doi:10.1006/mvre.1997.2045
2. Blanco R, Gerhardt H (2013) VEGF and Notch in tip and stalk cell selection. Cold Spring Harbor perspectives in medicine 3 (1):a006569. doi:10.1101/cshperspect.a006569
3. Vossenaar ER, Zendman AJ, van Venrooij WJ, Pruijn GJ (2003) PAD, a growing family of citrullinating enzymes: genes, features and involvement in disease. BioEssays : news and reviews in molecular, cellular and developmental biology 25 (11):1106-1118. doi:10.1002/bies.10357
4. Ferrara N, Gerber HP, LeCouter J (2003) The biology of VEGF and its receptors. Nat Med 9 (6):669-676. doi:10.1038/nm0603-669
5. Gerhardt H, Golding M, Fruttiger M, Ruhrberg C, Lundkvist A, Abramsson A, Jeltsch M, Mitchell C, Alitalo K, Shima D, Betsholtz C (2003) VEGF guides angiogenic sprouting utilizing endothelial tip cell filopodia. J Cell Biol 161 (6):1163-1177. doi:10.1083/jcb.200302047

6. Lobov I, Mikhailova N (2018) The Role of Dll4/Notch Signaling in Normal and Pathological Ocular Angiogenesis: Dll4 Controls Blood Vessel Sprouting and Vessel Remodeling in Normal and Pathological Conditions. J Ophthalmol 2018:3565292. doi:10.1155/2018/3565292
7. Kopan R, Ilagan MX (2009) The canonical Notch signaling pathway: unfolding the activation mechanism. Cell 137 (2):216-233. doi:10.1016/j.cell.2009.03.045
8. Benedito R, Roca C, Sorensen I, Adams S, Gossler A, Fruttiger M, Adams RH (2009) The notch ligands Dll4 and Jagged1 have opposing effects on angiogenesis. Cell 137 (6):1124-1135. doi:10.1016/j.cell.2009.03.025
9. Ziółkowska K, Kwapiszewski R, Brzózka Z (2011) Microfluidic devices as tools for mimicking the in vivo environment. New Journal of Chemistry 35 (5):979-990. doi:10.1039/C0NJ00709A
10. Bajaj P, Schweller RM, Khademhosseini A, West JL, Bashir R (2014) 3D biofabrication strategies for tissue engineering and regenerative medicine. Annual review of biomedical engineering 16:247-276. doi:10.1146/annurev-bioeng-071813-105155
11. Bai J, Wang C (2020) Organoids and Microphysiological Systems: New Tools for Ophthalmic Drug Discovery. Frontiers in Pharmacology 11 (407). doi:10.3389/fphar.2020.00407
12. Avendano A, Cortes-Medina M, Song JW (2019) Application of 3-D Microfluidic Models for Studying Mass Transport Properties of the Tumor Interstitial Matrix. Front Bioeng Biotechnol 7:6. doi:10.3389/fbioe.2019.00006
13. Motherwell J, Murfee WL (2018) Modelling microvascular pathology. Nat Biomed Eng 2 (6):349-350. doi:10.1038/s41551-018-0251-9
14. van Duinen V, Trietsch SJ, Joore J, Vulto P, Hankemeier T (2015) Microfluidic 3D cell culture: from tools to tissue models. Current opinion in biotechnology 35:118-126. doi:10.1016/j.copbio.2015.05.002
15. Kamm RD, Bashir R, Arora N, Dar RD, Gillette MU, Griffith LG, Kemp ML, Kinlaw K, Levin M, Martin AC, McDevitt TC, Nerem RM, Powers MJ, Saif TA, Sharpe J, Takayama S, Takeuchi S, Weiss R, Ye K, Yevick HG, Zaman MH (2018) Perspective: The promise of multi-cellular engineered living systems. APL Bioengineering 2 (4):040901. doi:10.1063/1.5038337
16. Andrejecsk JW, Hughes CCW (2018) Engineering perfused microvascular networks into microphysiological systems platforms. Current Opinion in Biomedical Engineering 5:74-81. doi:https://doi.org/10.1016/j.cobme.2018.02.002
17. Haase K, Kamm RD (2017) Advances in on-chip vascularization. Regen Med 12 (3):285-302. doi:10.2217/rme-2016-0152
18. Yeon JH, Ryu HR, Chung M, Hu QP, Jeon NL (2012) In vitro formation and characterization of a perfusable three-dimensional tubular capillary network in microfluidic devices. Lab on a Chip 12 (16):2815-2822. doi:10.1039/C2LC40131B
19. van Duinen V, Zhu D, Ramakers C, van Zonneveld AJ, Vulto P, Hankemeier T (2019) Perfused 3D angiogenic sprouting in a high-throughput in vitro platform. Angiogenesis 22 (1):157-165. doi:10.1007/s10456-018-9647-0
20. Zeinali S, Bichsel CA, Hobi N, Funke M, Marti TM, Schmid RA, Guenat OT, Geiser T (2018) Human microvasculature-on-a chip: anti-neovasculogenic effect of nintedanib in vitro. Angiogenesis 21 (4):861-871. doi:10.1007/s10456-018-9631-8
21. Bai J, Adriani G, Dang TM, Tu TY, Penny HX, Wong SC, Kamm RD, Thiery JP (2015) Contact-dependent carcinoma aggregate dispersion by M2a macrophages via ICAM-1 and beta2 integrin interactions. Oncotarget 6 (28):25295-25307. doi:10.18632/oncotarget.4716
22. Bai J, Tu TY, Kim C, Thiery JP, Kamm RD (2015) Identification of drugs as single agents or in combination to prevent carcinoma dissemination in a microfluidic 3D environment. Oncotarget 6 (34):36603-36614. doi:10.18632/oncotarget.5464
23. Aref AR, Huang RY, Yu W, Chua KN, Sun W, Tu TY, Bai J, Sim WJ, Zervantonakis IK, Thiery JP, Kamm RD (2013) Screening therapeutic EMT blocking agents in a three-dimensional microenvironment.

Integrative biology : quantitative biosciences from nano to macro 5 (2):381-389. doi:10.1039/c2ib20209c
24. Horbach S, Halffman W (2017) The ghosts of HeLa: How cell line misidentification contaminates the scientific literature. PloS one 12 (10):e0186281. doi:10.1371/journal.pone.0186281
25. Perez RA, Mestres G (2016) Role of pore size and morphology in musculo-skeletal tissue regeneration. Materials Science and Engineering: C 61:922-939. doi:https://doi.org/10.1016/j.msec.2015.12.087
26. Rohan RM, Fernandez A, Udagawa T, Yuan J, D'Amato RJ (2000) Genetic heterogeneity of angiogenesis in mice. FASEB journal : official publication of the Federation of American Societies for Experimental Biology 14 (7):871-876
27. Khajavi M, Zhou Y, Birsner AE, Bazinet L, Rosa Di Sant A, Schiffer AJ, Rogers MS, Krishnaji ST, Hu B, Nguyen V, Zon L, D'Amato RJ (2017) Identification of Padi2 as a novel angiogenesis-regulating gene by genome association studies in mice. PLoS genetics 13 (6):e1006848. doi:10.1371/journal.pgen.1006848
28. McElwee JL, Mohanan S, Griffith OL, Breuer HC, Anguish LJ, Cherrington BD, Palmer AM, Howe LR, Subramanian V, Causey CP, Thompson PR, Gray JW, Coonrod SA (2012) Identification of PADI2 as a potential breast cancer biomarker and therapeutic target. BMC Cancer 12:500. doi:10.1186/1471-2407-12-500
29. Koch MW, Metz LM, Kovalchuk O (2013) Epigenetic changes in patients with multiple sclerosis. Nat Rev Neurol 9 (1):35-43. doi:10.1038/nrneurol.2012.226
30. Tigges U, Welser-Alves JV, Boroujerdi A, Milner R (2012) A novel and simple method for culturing pericytes from mouse brain. Microvascular research 84 (1):74-80. doi:10.1016/j.mvr.2012.03.008
31. Perriere N, Demeuse P, Garcia E, Regina A, Debray M, Andreux JP, Couvreur P, Scherrmann JM, Temsamani J, Couraud PO, Deli MA, Roux F (2005) Puromycin-based purification of rat brain capillary endothelial cell cultures. Effect on the expression of blood-brain barrier-specific properties. Journal of neurochemistry 93 (2):279-289. doi:10.1111/j.1471-4159.2004.03020.x
32. Song JW, Munn LL (2011) Fluid forces control endothelial sprouting. Proceedings of the National Academy of Sciences of the United States of America 108 (37):15342-15347. doi:10.1073/pnas.1105316108
33. Chen MB, Hajal C, Benjamin DC, Yu C, Azizgolshani H, Hynes RO, Kamm RD (2018) Inflamed neutrophils sequestered at entrapped tumor cells via chemotactic confinement promote tumor cell extravasation. Proceedings of the National Academy of Sciences of the United States of America 115 (27):7022-7027. doi:10.1073/pnas.1715932115
34. Ludovica V. AS, Zdenko H., Rabih M. (2017) Mechanisms of Histone Modifications. In: Handbook of Epigenetics (Second edition). Academic Press, pp 25-46. doi:https://doi.org/10.1016/B978-0-12-805388-1.00003-1
35. Thurston G, Kitajewski J (2008) VEGF and Delta-Notch: interacting signalling pathways in tumour angiogenesis. Br J Cancer 99 (8):1204-1209. doi:10.1038/sj.bjc.6604484
36. Zhang X, Bolt M, Guertin MJ, Chen W, Zhang S, Cherrington BD, Slade DJ, Dreyton CJ, Subramanian V, Bicker KL, Thompson PR, Mancini MA, Lis JT, Coonrod SA (2012) Peptidylarginine deiminase 2-catalyzed histone H3 arginine 26 citrullination facilitates estrogen receptor alpha target gene activation. Proceedings of the National Academy of Sciences of the United States of America 109 (33):13331-13336. doi:10.1073/pnas.1203280109
37. Falcao AM, Meijer M, Scaglione A, Rinwa P, Agirre E, Liang J, Larsen SC, Heskol A, Frawley R, Klingener M, Varas-Godoy M, Raposo A, Ernfors P, Castro DS, Nielsen ML, Casaccia P, Castelo-Branco G (2019) PAD2-Mediated Citrullination Contributes to Efficient Oligodendrocyte Differentiation and Myelination. Cell Rep 27 (4):1090-1102 e1010. doi:10.1016/j.celrep.2019.03.108

38. Ostergaard L, Engedal TS, Moreton F, Hansen MB, Wardlaw JM, Dalkara T, Markus HS, Muir KW (2016) Cerebral small vessel disease: Capillary pathways to stroke and cognitive decline. J Cereb Blood Flow Metab 36 (2):302-325. doi:10.1177/0271678X15606723
39. Bodnar RJ, Rodgers ME, Chen WC, Wells A (2013) Pericyte regulation of vascular remodeling through the CXC receptor 3. Arteriosclerosis, thrombosis, and vascular biology 33 (12):2818-2829. doi:10.1161/ATVBAHA.113.302012
40. Bergers G, Song S (2005) The role of pericytes in blood-vessel formation and maintenance. Neuro Oncol 7 (4):452-464. doi:10.1215/S1152851705000232
41. Darrah E, Rosen A, Giles JT, Andrade F (2012) Peptidylarginine deiminase 2, 3 and 4 have distinct specificities against cellular substrates: novel insights into autoantigen selection in rheumatoid arthritis. Annals of the rheumatic diseases 71 (1):92-98. doi:10.1136/ard.2011.151712
42. Wang L, Song G, Zhang X, Feng T, Pan J, Chen W, Yang M, Bai X, Pang Y, Yu J, Han J, Han B (2017) PADI2-Mediated Citrullination Promotes Prostate Cancer Progression. Cancer research 77 (21):5755-5768. doi:10.1158/0008-5472.CAN-17-0150
43. Moscarello MA, Mastronardi FG, Wood DD (2007) The role of citrullinated proteins suggests a novel mechanism in the pathogenesis of multiple sclerosis. Neurochemical research 32 (2):251-256. doi:10.1007/s11064-006-9144-5
44. Guarani V, Deflorian G, Franco CA, Kruger M, Phng LK, Bentley K, Toussaint L, Dequiedt F, Mostoslavsky R, Schmidt MHH, Zimmermann B, Brandes RP, Mione M, Westphal CH, Braun T, Zeiher AM, Gerhardt H, Dimmeler S, Potente M (2011) Acetylation-dependent regulation of endothelial Notch signalling by the SIRT1 deacetylase. Nature 473 (7346):234-238. doi:10.1038/nature09917
45. Lobov IB, Renard RA, Papadopoulos N, Gale NW, Thurston G, Yancopoulos GD, Wiegand SJ (2007) Delta-like ligand 4 (Dll4) is induced by VEGF as a negative regulator of angiogenic sprouting. Proceedings of the National Academy of Sciences of the United States of America 104 (9):3219-3224. doi:10.1073/pnas.0611206104
46. Bai J, Fu H, Bazinet L, Birsner AE, D'Amato RJ (2020) A Method for Developing Novel 3D Cornea-on-a-Chip Using Primary Murine Corneal Epithelial and Endothelial Cells. Frontiers in Pharmacology 11 (453). doi:10.3389/fphar.2020.00453

Figure Legends

Fig.1 Microfluidic angiogenic platform using primary cells. a. Flow chart of mouse primary endothelial cells/pericyte isolation and induced in-device angiogenesis, red: endothelial cells (EC), green: pericytes (PC). b. Characterization of 129S1/SvlmJ mouse primary endothelial cells and pericytes via flow cytometry. The endothelial cells are defined as CD31+ (PE) and VEGFR2+ (PE) and PDGFRβ- (FITC); while pericytes are defined as positive for PDGFRβ (FITC), NG2 (Alexa fluor 488) and are negative for CD31 (PE), blue peaks are stained samples, and red peaks are unstained control. c. Immunofluorescent staining with counterstain on C57BL/6J and 129S1/SvlmJ mouse primary endothelial cells and pericytes (red: CD31; green: NG2; blue: nuclei). d. Phase-contrast image on C57BL/6J and 129S1/SvlmJ mouse primary endothelial cells and pericytes. e. Schematic of device design: overall layout of the media channels and gel regions where central region is used for introducing collagen gel; the two side channels for filling culture medium and growing endothelial cells/pericytes. An enlarged isometric view of the device on the right shows the relative locations of endothelial cells, pericytes and induced angiogenic vessel sprouts. The inset figure indicated a pericyte covers multiple endothelial cells and is migrating

along the vessel sprouts. Scale bars: 100 μm. f. Pericytes migration in angiogenesis. Scale bars: 50 μm

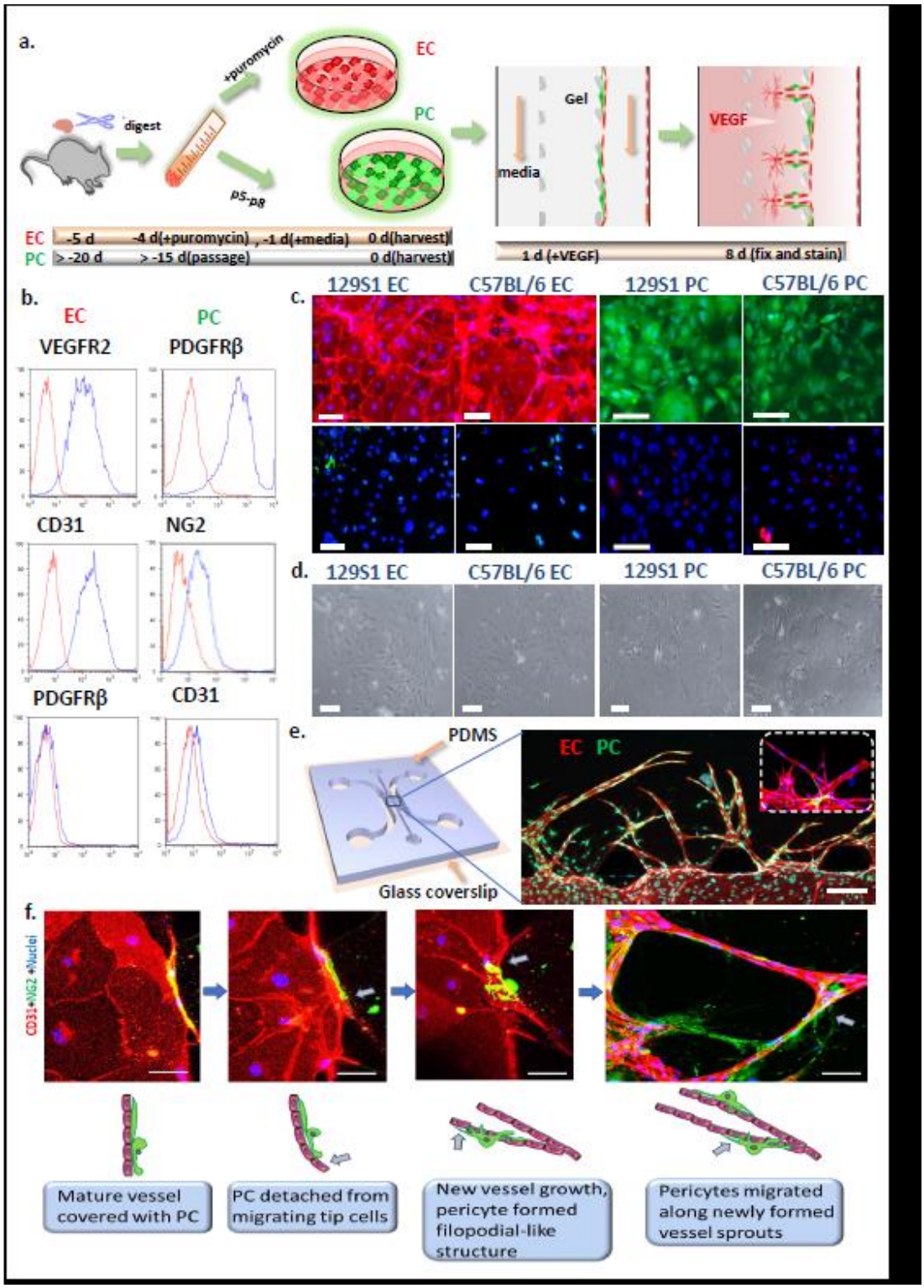

Fig.2 Comparison of Three-dimensional neovessels and microenvironment formed by

C57BL/6J and 129S1/SvlmJ cells in microfluidic device. a. Immunofluorescent staining of self-assembled vessel structure by co-culture of endothelial cells and pericytes. b. Immunofluorescent staining of angiogenic sprouts induced from C57BL/6J and 129S1/SvlmJ endothelial cells and pericytes coculture (red: CD31 stained endothelial cells; green: NG2 stained pericytes; blue: nuclei). Angiogenesis was induced by 25 ng/mL VEGF for 7 days. c. Quantitative analysis on angiogenic sprouting length for four groups: 129S1/SvlmJ endothelial cell culture only; 129S1/SvlmJ endothelial cells in coculture with 129S1/SvlmJ pericytes; C57BL/6J endothelial cell culture only; C57BL/6J endothelial cells in coculture with C57BL/6J pericytes. d. Quantitative analysis on tip cell numbers for four groups (as in c). e. Quantitative analysis on vessel diameters for four groups (as in c). f. Blood vessel lumen formation, pericyte adherence to and migration along the endothelial cell sprouts from a representative image (129S1/SvlmJ coculture). g. Concentration profiles and representative images at 0min and 5mins of fluorescent dextran from which permeability can be quantified, for endothelial cell only and endothelial cell-pericyte coculture. 129S1/SvlmJ. h. Quantitative analysis on the diffusion permeability across the vessel sprouts, for four groups (as in c). Average values across n = 10 regions within a single device. i. Schematic demonstration on endothelial cell sprouting and pericyte migration in two strains. j. Immunofluorescent staining on pericyte migration. k. Quantification on pericyte migration. Scale bars: 100 μm. Estimated diameter was obtained by dividing area of capillary sprouting by skeletal length. Tip regions were defined as the regions from the very tip to the first or second vascular loop.

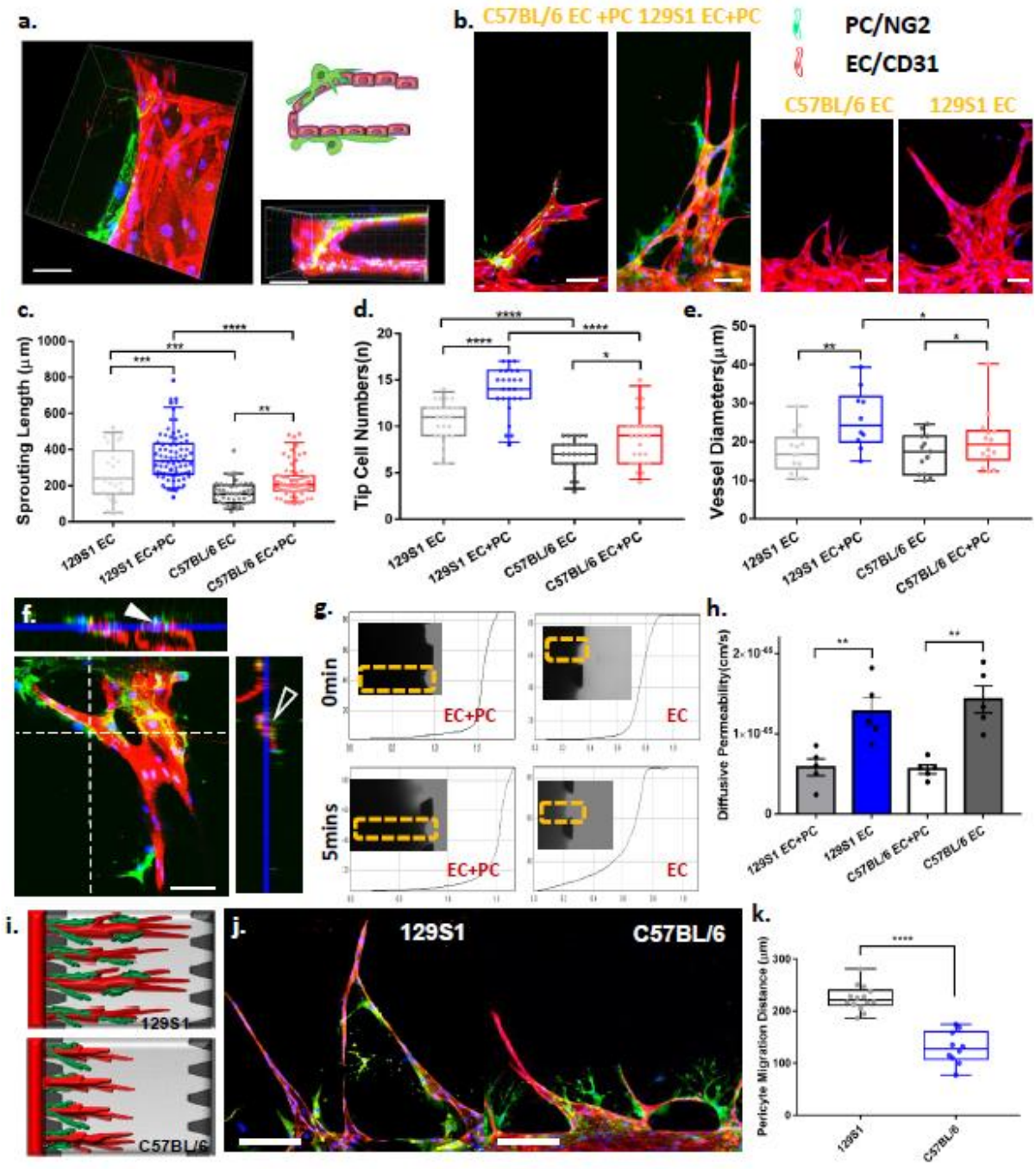

Fig.3 PADI2 expression on C57BL/6J and 129S1/SvlmJ coculture angiogenic microenvironment. a. PADI2 location and expression on endothelial cells and pericytes isolated from C57BL/6J and 129S1/SvlmJ mice in the presence of VEGF. Angiogenesis was induced by 25 ng/mL VEGF as described in Figure 2b. And enlarged angiogenic tip cell region with high expression of PADI2. b. PADI2 expression on endothelial cells and pericytes coculture in the absence of VEGF. Red: CD31; green: PADI2; magenta: NG2; blue: nuclei. Scale bars: 100 μm.

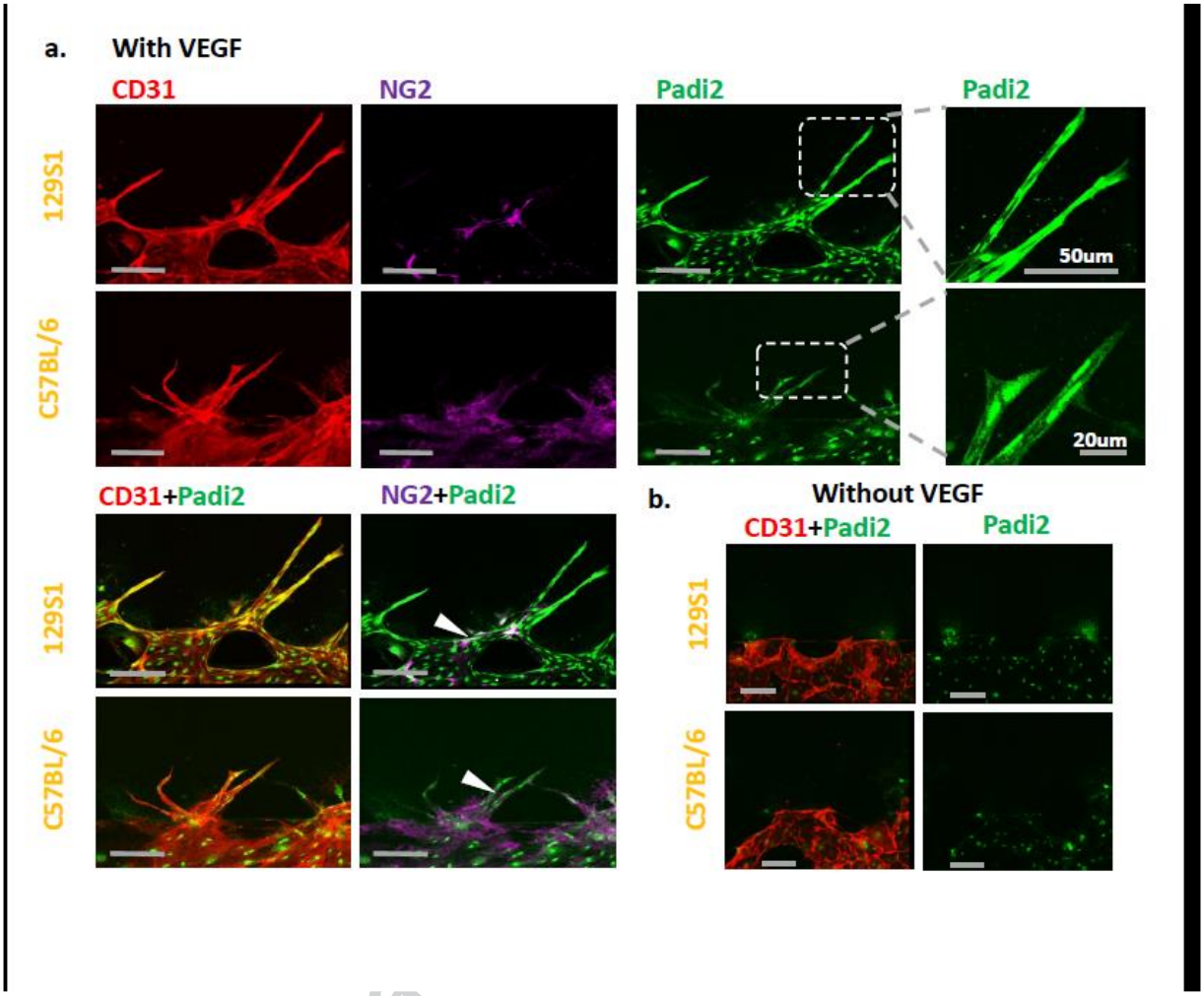

Fig.4 *Padi2* down-regulation or functional inhibition reduces angiogenesis. a. Western blot analysis on *Padi2* knock-down 129S1/SvlmJ endothelial cells via siRNA. b. Immunofluorescent staining of neovessel morphology, PADI2 and citrulline expression on vehicle versus *Padi2* knock-down (*Padi2* KD) group. c. Quantitative analysis on angiogenic sprouting length for vehicle and *Padi2* knock down (*Padi2* KD). d. Quantitative analysis on tip cell numbers for two groups (as in c). e. Quantitative analysis on vessel diameters for two groups (as in c). f. Effects of BB-Cl-Amidine inhibition on angiogenic sprouting. The angiogenic setup was treated by various doses (50 nM, 100 nM, 500 nM and 1000 nM) of BB-Cl-Amidine for 7 days with culture media changed every day. g. Quantitative analysis on angiogenic sprouting length for BB-Cl-Amidine treatment (dose response as in f). h. Quantitative analysis on tip cell numbers for or BB-Cl-Amidine treatment (dose response as in f). i. Quantitative analysis on vessel diameters for BB-Cl-Amidine treatment (dose response as in f). j. BB-Cl-Amidine inhibition on PADI2 function (2D). Endothelial cells were seeded in 24-well plate and treated by various doses (50 nM, 100 nM, 500 nM and 1000 nM) of BB-Cl-Amidine for 7 days with culture media changed every day. Red: CD31; green: PADI2; magenta: citrulline; blue: nuclei. k. Pericytes migration in the presence of BB-Cl-Amidine for both strains. Red: CD31; green: NG2; blue: nuclei. l. Quantification of k. Scale bars:

100 μm. Vehicle is the same sample subjected to electroporation but without carrying siRNA.

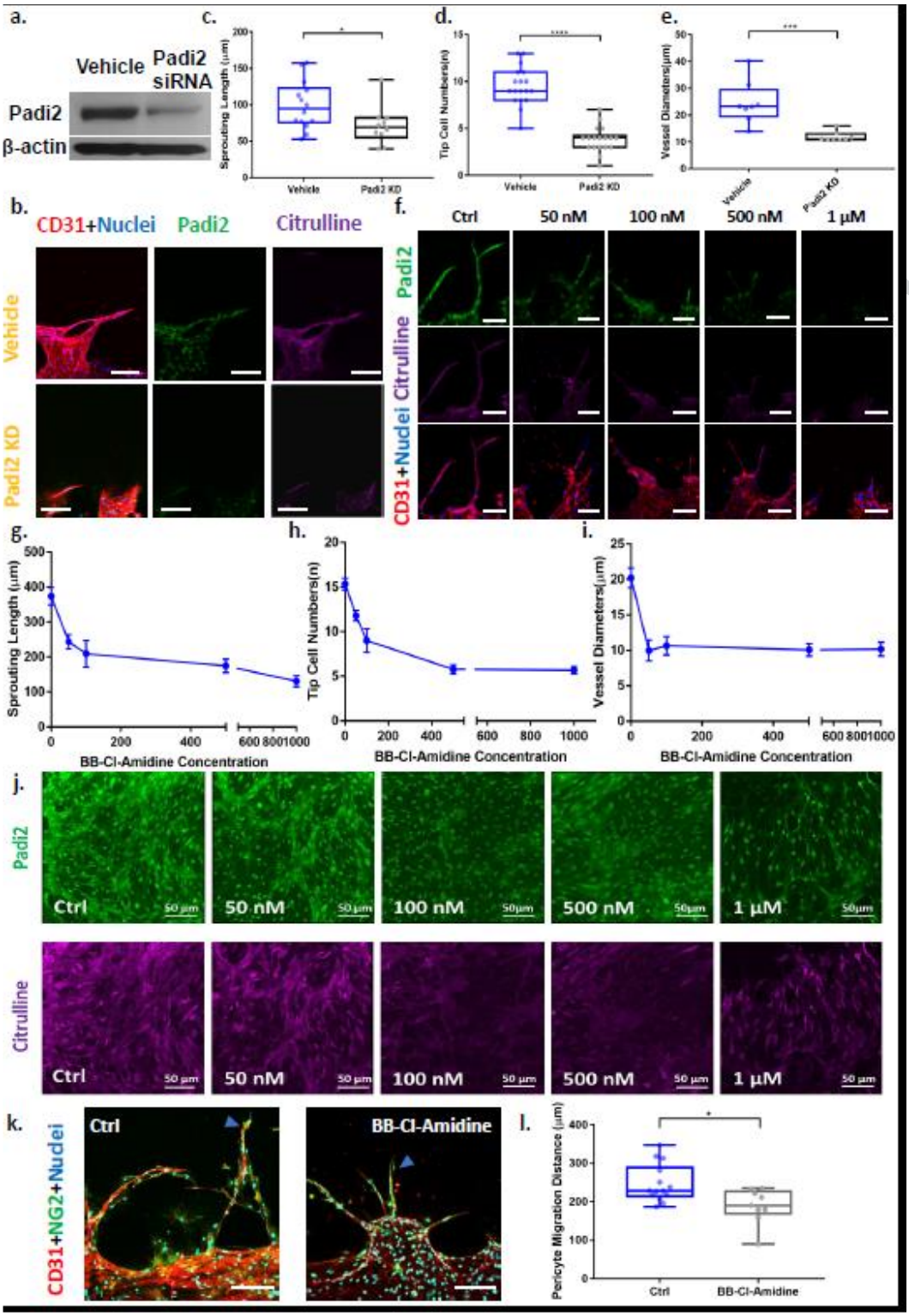

Fig.5 *Padi2* was negatively associated with Notch signaling in coculture. a. Immunofluorescent staining (with enlarged tip cell regions) of neovessel morphology and PADI2/citrulline expression

on C57BL/6J cells versus those cells treated by 20 μM DAPT. b. PADI2 expression on 129S1/SvlmJ cells versus those cells treated by 20 μM DAPT or 20 μM DAPT + 500 nM BB-Cl-Amidine. c. PADI2/citrulline expression on control versus 20 μM DAPT or 20 μM DAPT + 500nM BB-Cl-Amidine treatment groups within tip cell area (129S1/SvlmJ). White arrow indicates PADI2 accumulation on tip cell region. Red: CD31; green: PADI2; magenta: citrulline; blue: nuclei. Scale bars: 100 μm.

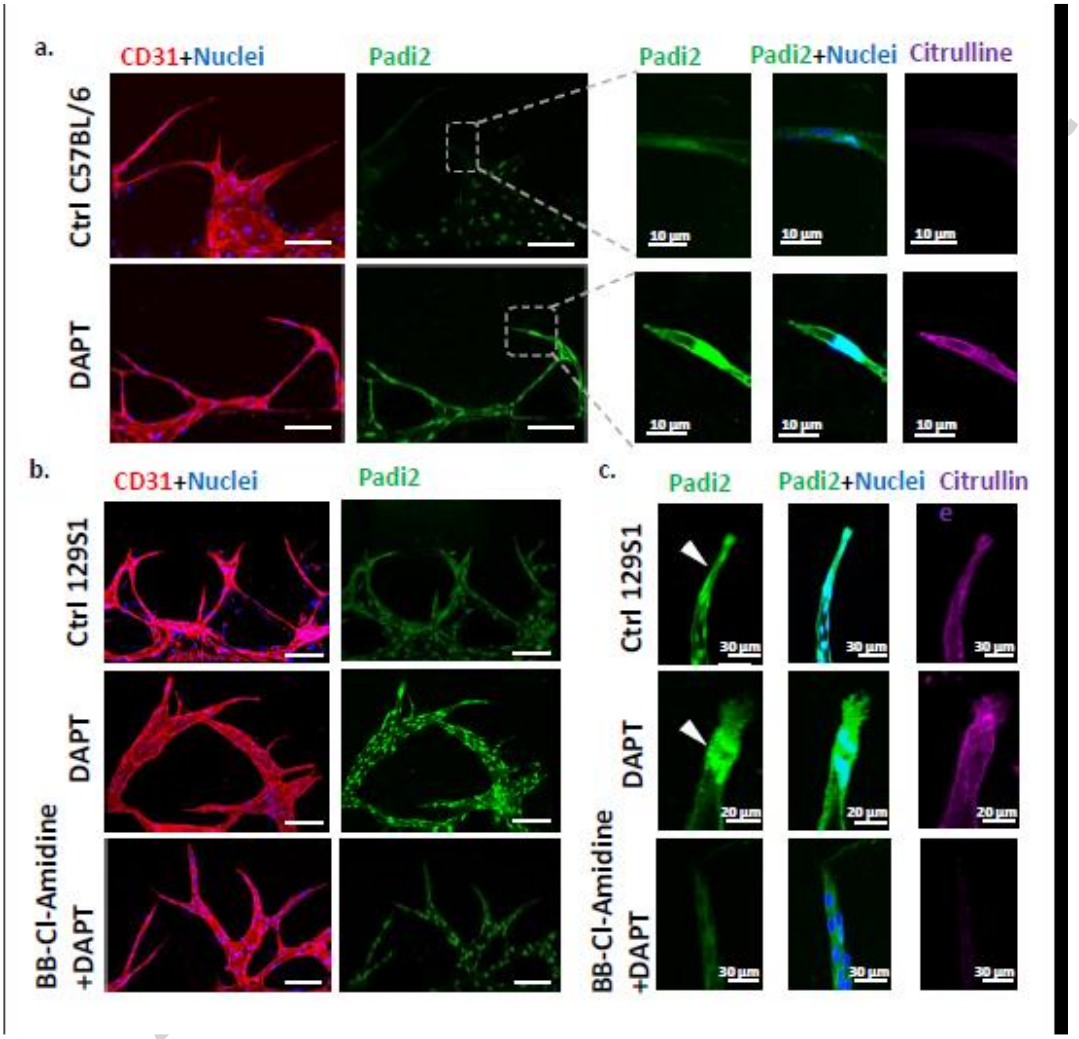

Fig.6 *Padi2* promotes angiogenesis through coordinated Notch signaling inhibition in coculture. a. *Notch1* intracellular domain (N1ICD) level with PADI2 functional (left) and expressional (right) inhibition. b. N1ICD nucleus level with PADI2 functional (up) and expressional inhibition (down). White arrow indicates nuclear N1ICD distribution (enlarged of a). c. Level of HEY1 and HEY2 with PADI2 expressional inhibition. d. HEY1 and HEY2 expressions on angiogenic vessel branches with PADI2 expressional inhibition (enlarged of c). e. Quantitative analysis on angiogenic sprouting length on control, 500 nM BB-Cl-Amidine, versus 20 μM DAPT + 500 nM BB-Cl-Amidine groups. f. Quantitative analysis on tip cell numbers for four groups (as in d). g. Quantitative analysis on vessel diameters for four groups (as in d). h. Neovessel

morphology for four groups (as in d). Red: CD31; green: HEY2; magenta: NOTCH1 intracellular domain (N1ICD); gray: HEY1; blue: nuclei. Scale bars: 100 μm.

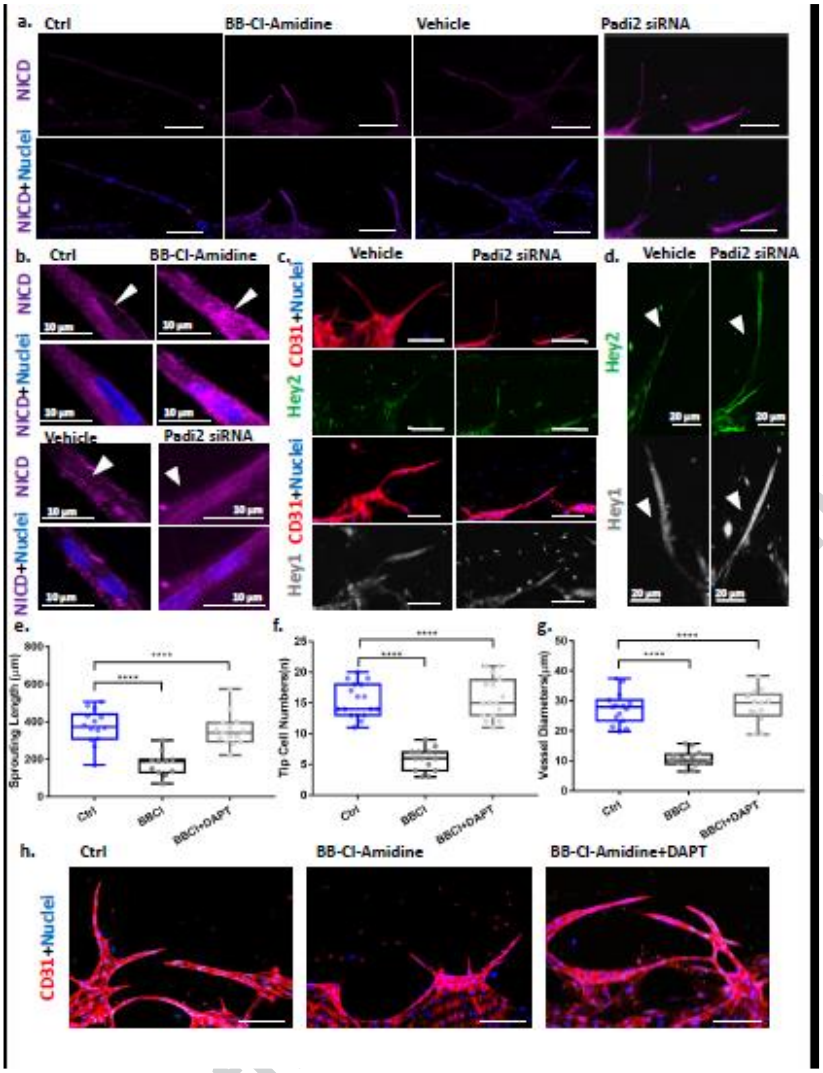

Fig.7 *Padi2* promotes angiogenesis through crosstalk with *Dll4/Notch1* signaling *in vitro*. a. Western blot analysis of DLL4, DLL1 and JAGGED1 expression on control versus 500 nM BB-Cl-Amidine treatment. b. Immunofluorescent images represent DLL4, DLL1 and JAGGED1 expression level on control versus BB-Cl-Amidine treatment. c. Neovessel morphology on control, BB-Cl-Amidine, DLL4 + BB-Cl-Amidine groups versus DLL4 + BB-Cl-Amidine + DAPT groups (500 nM BB-Cl-Amidine, 20 μM DAPT, 10 μg/mL recombinant mouse DLL4). d. Quantitative analysis on angiogenic sprouting length for four groups (as in c). e. Quantitative analysis on tip cell numbers for four groups (as in c). f. Quantitative analysis on vessel diameters for four groups (as in c). Red: CD31; green: DLL4; magenta: DLL1; gray: JAGGED1; blue: nuclei. Scale bars: 100 μm.